



Research article

Brain volumetric and fractal analysis of synthetic MRI: A comparative study with conventional 3D T1-weighted images

Sidong Liu^{a,b,1}, Tiebao Meng^{c,1}, Carlo Russo^a, Antonio Di Ieva^a, Shlomo Berkovsky^b,
Lingling Peng^d, Weiqiang Dou^d, Long Qian^{e,*}

^a Computational NeuroSurgery (CNS) Lab, Department of Clinical Medicine, Faculty of Medicine, Health and Human Sciences, Macquarie University, Sydney, Australia

^b Australian Institute of Health Innovation, Faculty of Medicine, Health and Human Sciences, Macquarie University, Sydney, Australia

^c Department of Radiology, Sun Yat-sen University Cancer Center, State Key Laboratory of Oncology in South China, Collaborative Innovation Center for Cancer Medicine, Guangzhou, China

^d MR Research, GE Healthcare, Beijing, China

^e Department of Biomedical Engineering, College of Engineering, Peking University, Beijing, China



ARTICLE INFO

Keywords:

Synthetic MRI
Brain volumetric analysis
Fractal analysis
Spatial resolution

ABSTRACT

Purpose: The estimation of brain volumetric measurements based on Synthetic MRI (SyMRI) is easy and fast, however, the consistency of brain volumetric and morphologic measurements based on SyMRI and 3D T1WI should be further addressed. The current study evaluated the impact of spatial resolution on brain volumetric and morphologic measurements using SyMRI, and test whether the brain measurements derived from SyMRI were consistent with those resulted from 3D T1WI.

Method: Brain volumetric and fractal analysis were applied to thirty healthy subjects, each underwent four SyMRI acquisitions with different spatial resolutions ($1 \times 1 \times 2$ mm, $1 \times 1 \times 3$ mm, $1 \times 1 \times 4$ mm, $2 \times 2 \times 2$ mm) and a 3D T1WI ($1 \times 1 \times 1$ mm isotropic). The consistency of the SyMRI measurements was tested using one-way non-parametric Kruskal-Wallis test and post hoc Dwass-Steel-Critchlow-Fligner test. The association between SyMRI and 3D T1WI derived measurements was evaluated using linear regression models.

Results: Our results demonstrated that both in- and through-plane resolutions show an impact on brain volumetric measurements, while brain parenchymal volume showed high consistency across the SyMRI acquisitions, and high association with the measurements from 3D T1WI. In addition, SyMRI with $1 \times 1 \times 4$ mm resolution showed the strongest association with 3D T1WI compared to other SyMRI acquisitions in both volumetric and fractal analyses. Moreover, substantial differences were found in fractal dimension of both gray and white matter between the SyMRI and 3D T1WI tissue segmentations.

Conclusions: Our results suggested that the measurements from SyMRI with relatively higher in-plane and lower through-plane resolution ($1 \times 1 \times 4$ mm) are much closer to 3D T1WI.

1. Introduction

Synthetic MRI (SyMRI) is a simulation technique for generating synthetic contrast-weighted images based on the measurement of tissue properties, such as the longitudinal R1 relaxation rate, the transverse R2 relaxation rate, and the proton density (PD) [1,2]. Previous studies have demonstrated that SyMRI enables easy and fast automatic brain tissue segmentation and volumetric analysis based on the quantification of R1, R2 and PD values [3,4]. SyMRI might be of clinical interest for the following reasons. First, SyMRI is inherently a multi-contrast imaging

technique; therefore, it is much faster to acquire a single session SyMRI than multi-session conventional MRI. This is particularly important when multi-modal MRI rather than T1-weighted MRI alone is required to assess diseases, such as multiple sclerosis [5,6] and brain tumors [7, 8]. Furthermore, using the SyMRI software, we can obtain multi-contrast images (e.g., T1-, T2-, PD-weighted images), various tissue segmentation maps (e.g., gray matter (GM), white matter (WM), cerebrospinal fluid (CSF) and myelin (MYE)) and quantitative volumetric measures (e.g., brain parenchymal volume (BPV) and intracranial volume (ICV)) in less than 1 min [9], allowing for a much faster

* Corresponding author at: Department of Biomedical Engineering, College of Engineering, Peking University, Beijing, 100871, China.

E-mail address: longqianad@gmail.com (L. Qian).

¹ These two authors contributed equally to this study.

<https://doi.org/10.1016/j.ejrad.2021.109782>

Received 10 January 2021; Received in revised form 23 April 2021; Accepted 18 May 2021

Available online 21 May 2021

0720-048X/© 2021 Elsevier B.V. All rights reserved.

analysis than the conventional T1-based analysis methods. In addition, SyMRI is able to produce myelin map which cannot be provided by T1-based segmentation methods. SyMRI has also shown more accurate segmentation compared to VBM8 and SPM12 using manual segmentations as references [10]. Indeed, SyMRI has been used in many clinical applications, such as the quantification of brain atrophy in neurodegenerative diseases [11,12] and longitudinal modeling of myelin content in pediatric brain development [13].

The preliminary clinical and research experiences have demonstrated the potential of SyMRI based brain segmentation approach; however, the consistency of brain volumetric and morphologic measurements based on SyMRI and 3D T1WI should be further addressed. Several studies have validated the SyMRI-based brain tissue segmentation and volumetry by comparisons with manual or automated methods [14–16]. Specifically, Vagberg et al. [15] compared the SyMRI tissue segmentations with both the manual and automated segmentation methods, while only the brain parenchymal fraction (BPF) was performed. Serai et al. [16] made the consistency analysis of GM, WM, CSF volumes between the SyMRI and 3D T1WI data, while the selection of spatial resolution of SyMRI acquisition was not taken into consideration. Previous study indicated that the significant volumetric differences were noted in most brain tissues when increasing the in-plane resolution from 0.8 mm to 3.6 mm [6]. Fujita et al. [14] compared the latest 3D SyMRI to the conventional 3D T1WI, and found that 3D SyMRI had a high scan-rescan repeatability and high agreement with T1WI producing reliable cortical thickness and volumetric measurements; however, the results could not extend to the 2D SyMRI and 3D T1WI due to the difference between 2D and 3D SyMRI sequences. Indeed, the FDA approved SyMRI is based on a 2D approach and has low through-plane resolution, the 3D SyMRI is under research and rarely reported (SyMRI refers to 2D SyMRI in current study without special indication). Hence, it is important to validate whether the SyMRI had the similar performance with the conventional 3D T1WI with 1.0 mm isotropic resolution in brain volumetric analysis.

In addition, previous studies [6,17] only demonstrated the impact of in-plane resolution on the volumetric analysis, yet the impact of slice thickness / spacing remains unknown. For 2D MRI sequences, there exists a wide range of choices of slice thickness, usually from 1 mm to 5 mm. When designing the imaging protocols for both research and clinical use, it is important to identify an optimal spatial resolution that can balance the trade-off between image acquisition / processing time and the analysis sensitivity. Furthermore, differences in spatial resolution could not only induce marked changes in volumetric measurements, but may also induce changes in the morphologic brain measurements, which have an important role in brain development and aging research [18], as well as in studies of the changes in brain structure associated with medical conditions, such as Alzheimer's disease [19] and schizophrenia [20]. The impact of spatial resolution in a broad sense, i.e., in-plane resolution and slice thickness / spacing, on brain morphology will need to be investigated, too.

Therefore, this study aims to investigate the impact of spatial resolution on the SyMRI-based brain volumetric and morphologic measurements, and test whether the brain measurements derived from SyMRI are consistent with those resulted from conventional 3D T1WI. To achieve our goals, in current study, volumetric and fractal analyses were performed to evaluate the differences in brain volumetric and morphologic measurements, respectively. Moreover, the consistency of four SyMRI acquisitions were evaluated and further compared them to the conventional 3D T1WI with 1.0 mm isotropic resolution as the reference.

2. Material and methods

2.1. Subjects

Thirty healthy subjects (15 males and 15 females; age: 24.6 ± 1.2)

were prospectively recruited in current study. None of the participants had a history of neurologic or psychiatric disease. This analysis was approved by the Institutional Review Board and written informed consent was obtained.

2.2. MRI protocol

A 3 T MRI system (Signa Pioneer, GE Healthcare) with a 32-channel head coil was used for image acquisition. Each participant underwent four SyMRI acquisitions with different spatial resolutions as shown in Table 1. For SyMRI, a two-dimensional multiple-dynamic multiple-echo (MDME) pulse sequence, comprising four automatically calculated saturation delay times and two echo times, was applied to acquire the axial sections. Detailed scan parameters for the MDME sequences were as follows: TR range, 10,000 ms; TE, 21 and 95 ms; FOV, 25.6 cm; echo train length, 16; bandwidth = 35.71 Hz; acceleration factor = 2; NEX = 1. Default TE / TR values (10 ms/650 ms) were used for T1W SyMRI reconstruction. We further acquired 3D T1WI data on the same cohort using the fast spoiled gradient recalled echo (FSPGR) sequence. Detailed scan parameters for the 3D T1WI sequence were as follows: TR/TE/TI = 7.5/3.1/450 ms; FA = 12°; FOV = 25.6; Matrix size = 256 × 256; Slice thickness = 1 mm; Acceleration factor = 2; NEX = 1. No fat saturation was applied. The scan time was approximately 5 min. All synthetic and 3D T1WI data were virtually examined for artefacts such as ring, blurring, and ghosting on site upon image acquisition. Images exhibiting these common artefacts were excluded and subjects with such artefacts were rescanned.

2.3. Brain volumetric analysis

For SyMRI acquisitions, the segmentation and volume estimation of the brain tissues, including WM, GM, CSF, NON, and myelin (MYE) were generated automatically using the SyMRI software (v8.0.4, SyntheticMR, Linköping, Sweden). The BPV was calculated as the sum of WM, GM and NON and the ICV was calculated as the sum of BPV and CSF [21, 22]. Fig. 1 shows an example of the brain tissue segmentations derived from a subject using different SyMRI acquisitions. For T1WI data, FreeSurfer (v6.0.0, <http://surfer.nmr.mgh.harvard.edu>) generated four measurements matching the SyMRI measurements: cerebral WM volume, total GM volume, brain segmentation volume and the estimated total ICV. Therefore, only these four measurements were compared between T1WI and SyMRI.

2.4. Fractal analysis

Fractal analysis has recently emerged as a quantitative tool in neuroscience, which offers a mathematical assessment of the morphological features, e.g., roughness and geometric complexity, of the brain [23–25]. Fractal dimension (FD), which is one of the most important parameters used in fractal analysis, quantifies the morphological self-similarity of objects and has been applied in neuroimaging research and clinical applications, such as, the assessment of brain tumors [26], multiple sclerosis [27], arteriovenous malformations [28], and structural brain complexity [29]. In our study, FD was computed and used as an objective measure to compare the morphometry of WM and GM obtained from different MRI sequences and SyMRI resolutions. The method for calculating the WM and GM FD was based on the 3D Box Counting algorithm, which is consistent with previous studies [27,28], using the following parameters: minimum box size of 1 mm and maximum box of 100 mm.

2.5. Statistical analysis

To investigate the repeatability of the synthetic MRI, we first performed the Shapiro-Wilk test [30] to assess the normality of the data, and further performed the one-way non-parametric analysis of variance

Table 1
Acquisition information of the SyMRI with different spatial resolutions.

| acquisitions | in-plane resolution (mm) | slice thickness (mm) | slice spacing (mm) | acquisition matrix | number of slices | acquisition time |
|--------------------------|--------------------------|----------------------|--------------------|--------------------|------------------|------------------|
| $1 \times 1 \times 2$ mm | 1.0×1.0 | 2.0 | 2.0 | 256×256 | 72 | 11 min 20 s |
| $1 \times 1 \times 3$ mm | 1.0×1.0 | 3.0 | 3.0 | 256×256 | 48 | 7 min 29 s |
| $1 \times 1 \times 4$ mm | 1.0×1.0 | 4.0 | 4.0 | 256×256 | 36 | 5 min 40 s |
| $2 \times 2 \times 2$ mm | 2.0×2.0 | 2.0 | 2.0 | 128×128 | 72 | 5 min 28 s |

$1 \times 1 \times 2$ mm: Synthetic MRI with $1 \times 1 \times 2$ mm resolution; $1 \times 1 \times 3$ mm: Synthetic MRI with $1 \times 1 \times 3$ mm resolution; $1 \times 1 \times 4$ mm: Synthetic MRI with $1 \times 1 \times 4$ mm resolution; $2 \times 2 \times 2$ mm: Synthetic MRI with $2 \times 2 \times 2$ mm resolution.

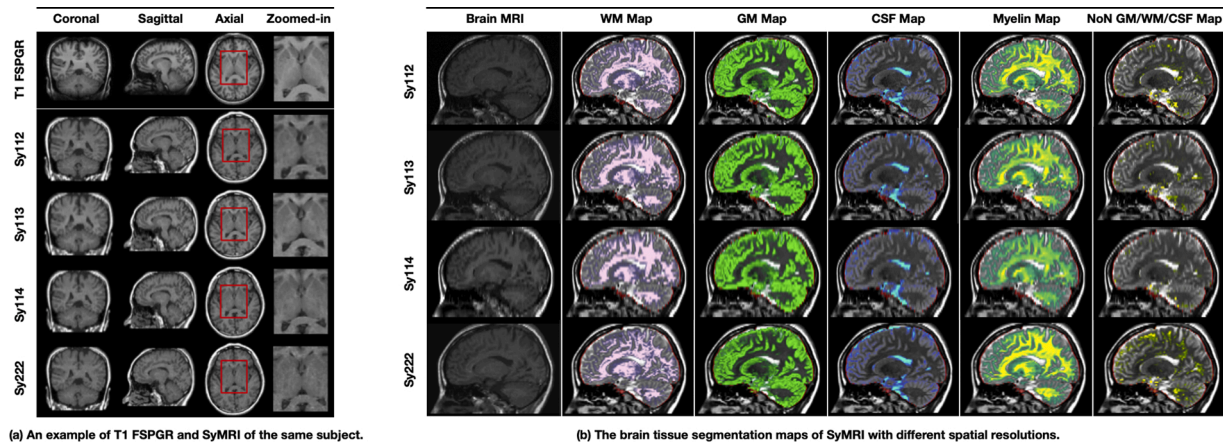


Fig. 1. (a) Comparison of T1 FSPGR and SyMRI of the same subject in different views, including coronal, sagittal, axial (the source), and the zoomed-in axial views. (b) The synthetic T_1 -weighted MRI and the brain tissue segmentation maps (WM, GM, CSF, NON and MYE) acquired from a subject with four different SyMRI acquisitions including $1 \times 1 \times 2$ mm, $1 \times 1 \times 3$ mm, $1 \times 1 \times 4$ mm and $2 \times 2 \times 2$ mm resolutions.

(ANOVA) using the Kruskal-Wallis test [31] to validate that the samples follow the same distribution. If the p -value suggested rejection of the null hypothesis that the population medians of all the groups were equal, then the post hoc pair-wise Dwass-Steel-Critchlow-Fligner (DSCF) tests [32] were performed to identify the groups that differed in their medians. A two-sided p -value $< .05$ was considered significant.

To compare the SyMRI acquisitions with T1WI, linear regression model and R^2 values were used to evaluate the correlation between the volumetric measurements extracted from different acquisitions (perfect association $R^2 = 1$; strong association $R^2 > 0.8$; meaningful association: $R^2 > 0.5$; no association $R^2 = 0$). All the test methods and the linear regression model were implemented in the SciPy (<https://www.scipy.org/>) and scikit-posthocs packages (<https://pypi.org/project/scikit-posthocs/>).

3. Results

3.1. Impact of spatial resolution

The distributions of the volumetric and morphologic measurements derived from the four SyMRI acquisitions are shown in Fig. 2. With different colors indicating different subjects. Most distributions passed the Shapiro-Wilk normality test, except for the CSF volumes ($p < .01$ for $1 \times 1 \times 2$ mm, $1 \times 1 \times 3$ mm and $1 \times 1 \times 4$ mm; $p < .05$ for $2 \times 2 \times 2$ mm) and the NON ($p < .001$ for $2 \times 2 \times 2$ mm). Although CSF and NON volumes failed the normality test, they were included in the following analysis using the Kruskal-Wallis and DSCF tests, which support both normal and non-normal distributions.

The Kruskal-Wallis and DSCF test results on the SyMRI volumetric measurements are shown in Table 2. No significant differences were found in the CSF volume, BPV and ICV using the one-way non-parametric Kruskal-Wallis test. However, significant differences were found in WM ($p < .05$), GM ($p < .05$), NON ($p < .001$) and MYE ($p < .01$) volumes. The post hoc analysis of these measurements using the DSCF

test suggested that the differences were mostly found between SyMRI with $2 \times 2 \times 2$ mm resolution and other acquisitions ($2 \times 2 \times 2$ mm vs. $1 \times 1 \times 4$ mm in GM and MYE volumes; $2 \times 2 \times 2$ mm vs. all the other SyMRI acquisitions in NON volumes). We also found moderate but significant difference between SyMRI with $1 \times 1 \times 2$ mm and $1 \times 1 \times 4$ mm resolutions in NON and MYE volumes ($p < .05$).

We further tested the differences in morphologic measurements between different SyMRI acquisitions. Table 3 shows the results of the Kruskal-Wallis and DSCF tests on WM- and GM-FD values. No significant differences were found between SyMRI acquisitions in WM or GM morphology.

3.2. Comparison with T1-weighted MRI

Fig. 3 shows the scatter plots of the volumetric measurements derived from SyMRI against those from T1WI. The linear trend lines are also plotted with R^2 values indicating the degree of association between variables.

All the SyMRI acquisitions showed positive correlation with T1WI, achieving the strongest agreement in BPV (R^2 range: 0.89 – 0.96), followed by ICV, which also showed strong and almost strong association (R^2 range: 0.76 – 0.80). However, there was a high variability between the SyMRI and T1WI in the WM volume (R^2 range: 0.44 – 0.87) and GM volume (R^2 range: 0.44 – 0.80).

Overall SyMRI with $1 \times 1 \times 4$ mm resolution achieved the highest association with T1WI on the WM volume ($R^2 = 0.87$), GM volume ($R^2 = 0.80$) and BPV ($R^2 = 0.96$); and SyMRI with $2 \times 2 \times 2$ mm resolution, on the contrary, had the lowest association with T1WI on these measurements. We note that SyMRI with $2 \times 2 \times 2$ mm resolution achieved the highest association with T1WI on ICV ($R^2 = 0.80$), but the R^2 difference to other SyMRI acquisitions was only marginal.

Fig. 4 shows the scatter plots of the morphologic measurements derived from SyMRI against those from T1WI. The GM-FD (R^2 range: 0.44 – 0.72) was preserved better than the WM-FD (R^2 range: 0.14 –

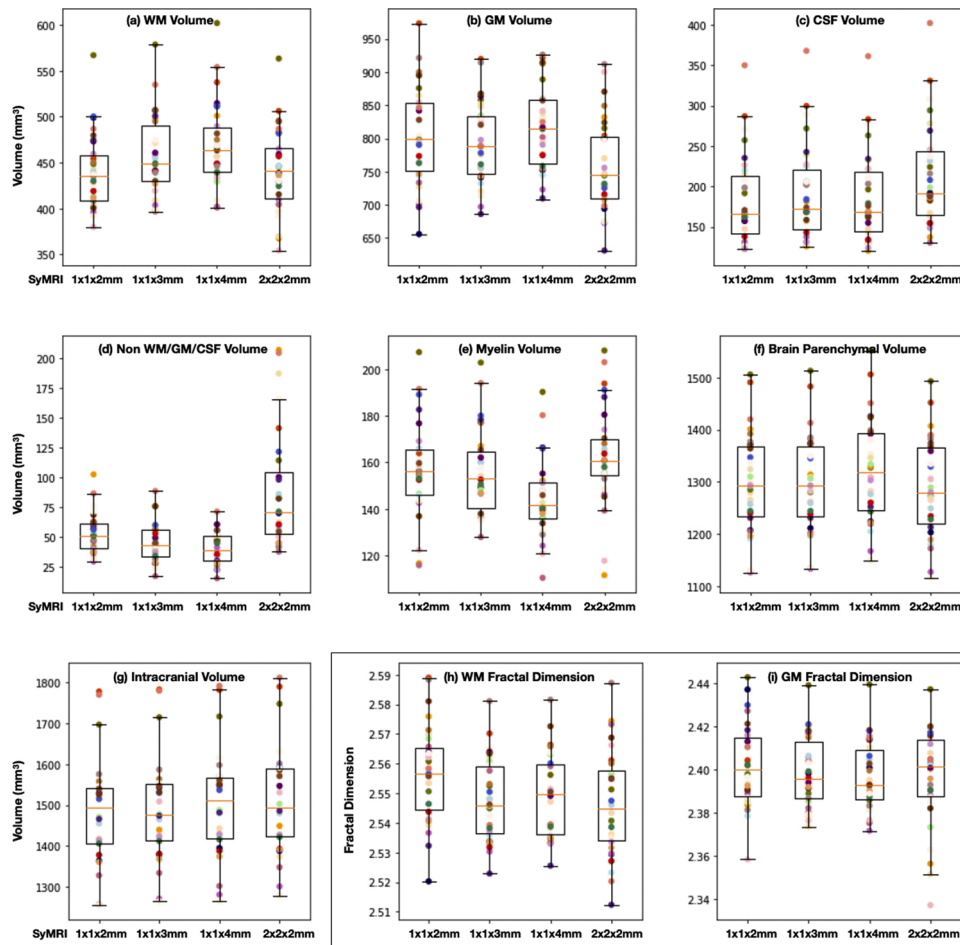


Fig. 2. Distributions of the brain volumetric measurements (a-g) and morphologic measurements (h, i) derived from four SyMRI acquisitions.

0.67) in SyMRI acquisitions; however, neither of them showed strong association with T1WI. SyMRI with $1 \times 1 \times 4$ mm resolution again showed the highest association with T1WI, whereas SyMRI with $2 \times 2 \times 2$ mm resolution had the lowest association with T1WI in both WM-FD and GM-FD.

4. Discussion

Volumetric MRI protocols have been recommended to assess neuro-inflammatory and -degenerative conditions [19,33]. Indeed, SyMRI has been used in the quantification of brain atrophy in multiple sclerosis [5, 6] and Alzheimer's diseases [11,12]. In particular, SyMRI enables the quantification of myelin content, which is a key component of the central nervous system, facilitating electrical conduction in neural circuits and providing trophic support for axons [22]. Myelination is the last stage of WM development, and delayed myelination is shown in children with development delay [13]. It would be a very good use case for SyMRI to provide more types of tissue maps as well as more accurate and faster volumetric and morphological measures to assist these research and clinical applications.

In this study, we tested the consistency of SyMRI acquisitions with different spatial resolutions and compared them to the conventional T1WI in volumetric and fractal analyses. Among all the tested volumetric measurements, BPV showed high consistency across the SyMRI acquisitions, and high association with the T1WI measurements, implying a potential of SyMRI in brain development and aging research and the assessment of neurodegenerative and neuro-inflammatory disorders [19,33]. SyMRI with $1 \times 1 \times 4$ mm resolution showed the strongest association with T1WI in both volumetric and fractal analyses.

However, substantial morphological differences were found between SyMRI and T1WI when comparing their tissue segmentations, indicating that the SyMRI based on 2D MDME sequence and the 3D T1-FSPGR could not produce comparable results with the FD-based morphological assessment used in this study.

Among the four distinct SyMRI acquisitions, no significant differences were found in the CSF volume, BPV and ICV, or in WM-FD and GM-FD, which indicates high consistency of these measurements and robustness of SyMRI for various spatial resolutions. However, significant differences were observed between SyMRI with $2 \times 2 \times 2$ mm resolution and other SyMRI acquisitions in WM ($p < .05$), GM ($p < .05$), NON ($p < .001$) and MYE ($p < .01$) volumes, demonstrating the impact of in-plane resolution ($2 \times 2 \times 2$ mm vs. 1×1 mm) on the volumetric measurements – the $2 \times 2 \times 2$ mm protocol was at least twice the volume of the other evaluated SyMRI protocols. This finding aligns with previous studies [6,17]. We further identified moderate but significant differences in NON and MYE volumes when comparing SyMRI with $1 \times 1 \times 2$ mm and $1 \times 1 \times 4$ mm resolutions, which implies that the changes in slice thickness / spacing are an important factor in brain volumetric analyses and may induce substantial differences to the analysis results. Lower associations in the FD values between different acquisitions show that whereby loss of small details does not significantly impact the total volume amount, the computation of irregularity and roughness of the WM and GM can be affected in a considerable way.

All the SyMRI acquisitions showed positive correlation with T1WI in both volumetric and fractal analyses, and consistently achieved a high association with T1WI in BPV ($R^2 > 0.89$) and ICV ($R^2 > 0.75$). With regard to BPV, the results of both high consistency across the SyMRI acquisitions, and association with the T1WI implies a strong potential

Table 2
Kruskal-Wallis and DSCF test results on SyMRI volumetric measures.

| Volume | Kruskal-Wallis Test | Pairwise Comparison using DSCF Test | | | |
|--------|---------------------|-------------------------------------|-----------|--------------|--------------|
| | | | 1 × 1x3mm | 1 × 1 × 4 mm | 2 × 2 × 2 mm |
| WMV | 0.03* | 1 × 1 × 2 mm | 0.49 | 0.06 | 0.90 |
| | | 1 × 1x3mm | – | 0.73 | 0.73 |
| | | 1 × 1 × 4 mm | – | – | 0.20 |
| GMV | 0.01* | 1 × 1 × 2 mm | 1 × 1x3mm | 1 × 1 × 4 mm | 2 × 2 × 2 mm |
| | | 1 × 1x3mm | 0.90 | 0.90 | 0.13 |
| | | 1 × 1 × 4 mm | – | 0.74 | 0.25 |
| CSF | 0.20 | 1 × 1 × 2 mm | – | – | 0.02* |
| | | 1 × 1x3mm | 1 × 1x3mm | 1 × 1 × 4 mm | 2 × 2 × 2 mm |
| | | 1 × 1 × 4 mm | 0.90 | 0.90 | 0.34 |
| NON | <.001*** | 1 × 1 × 2 mm | – | 0.90 | 0.63 |
| | | 1 × 1x3mm | 0.42 | 0.03* | 0.44 |
| | | 1 × 1 × 4 mm | – | 0.77 | 0.01* |
| MYE | 0.002** | 1 × 1 × 2 mm | 1 × 1x3mm | 1 × 1 × 4 mm | 2 × 2 × 2 mm |
| | | 1 × 1x3mm | 0.90 | 0.04* | 0.67 |
| | | 1 × 1 × 4 mm | – | 0.17 | 0.52 |
| BPV | 0.55 | 1 × 1 × 2 mm | – | – | 0.001** |
| | | 1 × 1x3mm | 1 × 1x3mm | 1 × 1 × 4 mm | 2 × 2 × 2 mm |
| | | 1 × 1 × 4 mm | 0.90 | 0.87 | 0.90 |
| ICV | 0.57 | 1 × 1 × 2 mm | – | – | 0.90 |
| | | 1 × 1x3mm | 1 × 1x3mm | 1 × 1 × 4 mm | 2 × 2 × 2 mm |
| | | 1 × 1 × 4 mm | 0.90 | 0.83 | 0.78 |
| | | | – | – | 0.86 |
| | | | – | – | 0.90 |

WMV: white matter volume; GMV: gray matter volume; CSF: cerebrospinal fluid; NON: non-white matter/gray matter/CSF tissue; MYE: myelin; BPV: brain parenchymal volume; ICV: intracranial volume. 1 × 1 × 2 mm: Synthetic MRI with 1 × 1 × 2 mm resolution; 1 × 1x3mm: Synthetic MRI with 1 × 1x3mm resolution; 1 × 1 × 4 mm: Synthetic MRI with 1 × 1 × 4 mm resolution; 2 × 2 × 2 mm: Synthetic MRI with 2 × 2 × 2 mm resolution. **p* < 0.05; ***p* < 0.01; ****p* < 0.001.

Table 3
Kruskal-Wallis and DSCF test results on WM and GM FD values of SyMRI.

| Fractal Dimension | Kruskal-Wallis Test | Pairwise Comparison using DSCF Test | | | |
|-------------------|---------------------|-------------------------------------|-----------|--------------|--------------|
| | | | 1 × 1x3mm | 1 × 1 × 4 mm | 2 × 2 × 2 mm |
| WM-FD | 0.06 | 1 × 1 × 2 mm | 0.15 | 0.25 | 0.16 |
| | | 1 × 1x3mm | – | 0.90 | 0.90 |
| | | 1 × 1 × 4 mm | – | – | 0.90 |
| GM-FD | 0.78 | 1 × 1 × 2 mm | 1 × 1x3mm | 1 × 1 × 4 mm | 2 × 2 × 2 mm |
| | | 1 × 1x3mm | 0.90 | 0.82 | 0.90 |
| | | 1 × 1 × 4 mm | – | 0.90 | 0.90 |
| | | | – | – | 0.90 |

WM-FD: white matter-fractional dimension; GM-FD: gray matter-fractional dimension; DSCF: Dwass-Steel-Critchlow-Fligner test; 1 × 1 × 2 mm: Synthetic MRI with 1 × 1 × 2 mm resolution; 1 × 1x3mm: Synthetic MRI with 1 × 1x3mm resolution; 1 × 1 × 4 mm: Synthetic MRI with 1 × 1 × 4 mm resolution; 2 × 2 × 2 mm: Synthetic MRI with 2 × 2 × 2 mm resolution.

for the use of SyMRI in BPV-related research and clinical applications [34–36]. In addition, the highest association was found between SyMRI with 1 × 1 × 4 mm resolution and T1WI, which might be explained by the trade-off between the signal to noise ratio (SNR) and the slice thickness [37]. As the slice thickness increases from 2 mm/3 mm–4 mm, the R^2 values for WMV, GMV, WM-FD and GM-FD also increases. The 1 × 1 × 4 mm resolution is indeed the manufacturer suggested protocol, implying that SNR might have been a contributing factor of the default scanner protocol. However, there is high variability in WM and GM measurements across the SyMRI acquisitions compared to T1WI, e.g., marked differences were found between SyMRI with 1 × 1 × 4 mm resolution and T1WI as well as SyMRI with 2 × 2 × 2 mm resolution and T1WI in the WM volume (0.87 vs. 0.44), GM volume (0.80 vs. 0.44), WM-FD (0.67 vs. 0.14) and GM-FD (0.72 vs. 0.44). Such a high variability indicates a strong impact of spatial resolution on the volumetric and morphologic analysis, which further evidences our above-mentioned findings. Further, the SyMRI software can produce tissue segmentations with very short processing time (16 s), while it takes FreeSurfer 8 h to segment the tissues from T1WI and quantify the tissue volume on a powerful workstation with Intel Core i9–8950 CPU

and 32GB memory. Therefore, SyMRI, in the cases that multi-contrast weighted images are needed, may save time for image acquisition, and also reduce the time for tissue segmentation and volumetric analysis.

The relatively low association between SyMRI and T1WI in fractal analysis further indicates that there is a substantial difference between the SyMRI tissue segmentations and the FreeSurfer generated segmentations. The differences in the WM and GM segmentations may be attributable to three reasons. Firstly, in this study, the T1WI used an isotropic resolution of 1 mm, which was higher than that of the SyMRI acquisitions; therefore, the T1WI might have captured more structural details of the brain. Secondly, the tissue components from SyMRI and T1WI were computed differently. For SyMRI, the tissue ratio in each voxel was computed based on a predefined lookup grid to relate the tissue type to the $R_1 - R_2 - PD$ space [21,22], whereas the tissue segmentations from T1WI were calculated based on the voxel intensity using FreeSurfer. In addition, the NON component in SyMRI, is not captured by FreeSurfer and its anatomical basis and physiological implication is still unclear. Thirdly, as demonstrated by Fujita et al. [14], FreeSurfer could be applied to SyMRI; however, they only used FreeSurfer for cortical thickness analysis, and their SyMRI used a higher

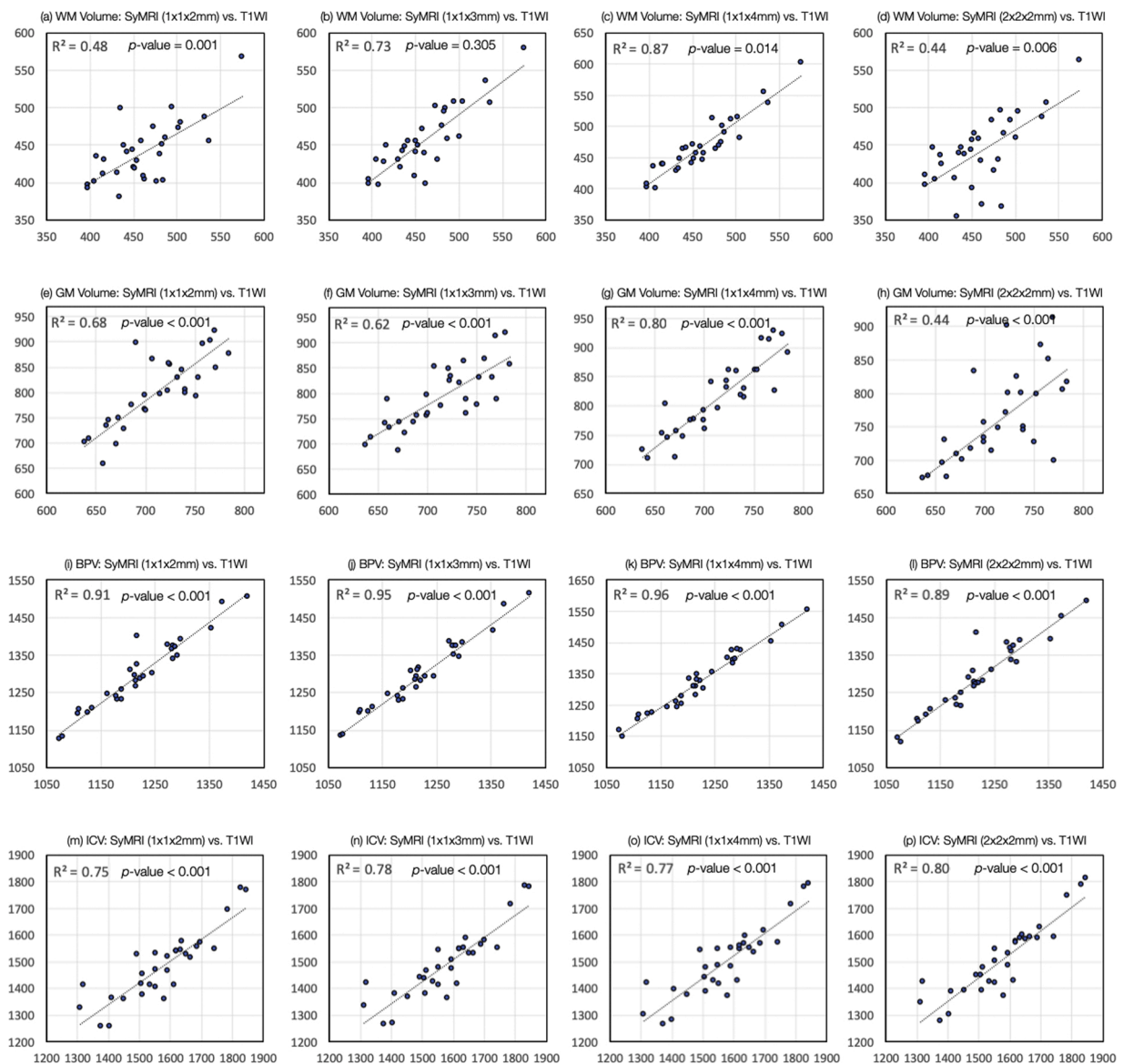


Fig. 3. Scatterplots of volumetric measurements from SyMRI compared with conventional T₁-weighted MRI. (a-d): WM volume; (e-h): GM volume; (i-l): BPV; (m-p): ICV.

resolution (isotropic 1 mm) than the sequences used in this study. Due to the limitation of the algorithm and the poor contrast between GM and WM in the brainstem, FreeSurfer tends to produce larger WMV than SyMRI. We therefore chose to not use FreeSurfer or other popular segmentation methods on SyMRI, such as FSL [38], SPM [39], ANTs [40], on SyMRI in order not to lose the inherent advantage of SyMRI in automated tissue segmentation.

Although our current study highlighted some key results, several limitations were noteworthy. First, a limited sample size was applied, which may influence the statistical power of our data. Second, our results were derived from a 3.0 T MRI scanner in one site, multi-site large dataset acquired from both 1.5 and 3 T MRI scanners should be considered in future. Last but not least, our current study was focused on healthy subjects, future studies should take the patients into consideration, and investigate its clinical diagnosis value.

5. Conclusions

In conclusion, our results suggested that the SyMRI with relatively higher in-plane and lower through-plane resolution ($1 \times 1 \times 4$ mm) may

have higher clinical applicability due to its higher SNR and shorter acquisition time; and also its volumetric and morphological measurements are much closer to conventional 3D T1WI.

CRedit authorship contribution statement

Sidong Liu: Formal analysis, Visualization, Writing - original draft, Writing - review & editing, Supervision, Funding acquisition. **Tiebao Meng:** Data curation, Resources, Writing - original draft. **Carlo Russo:** Validation, Formal analysis. **Antonio Di Ieva:** Validation, Funding acquisition. **Shlomo Berkovsky:** Formal analysis. **Lingling Peng:** Data curation, Software. **Weiqiang Dou:** Software. **Long Qian:** Conceptualization, Formal analysis, Methodology, Writing - review & editing, Supervision.

Declaration of Competing Interest

Lingling Peng and Weiqiang Dou are employees of GE Healthcare. The other authors declare that they have no known competing financial interests or personal relationships that could have appeared to influence

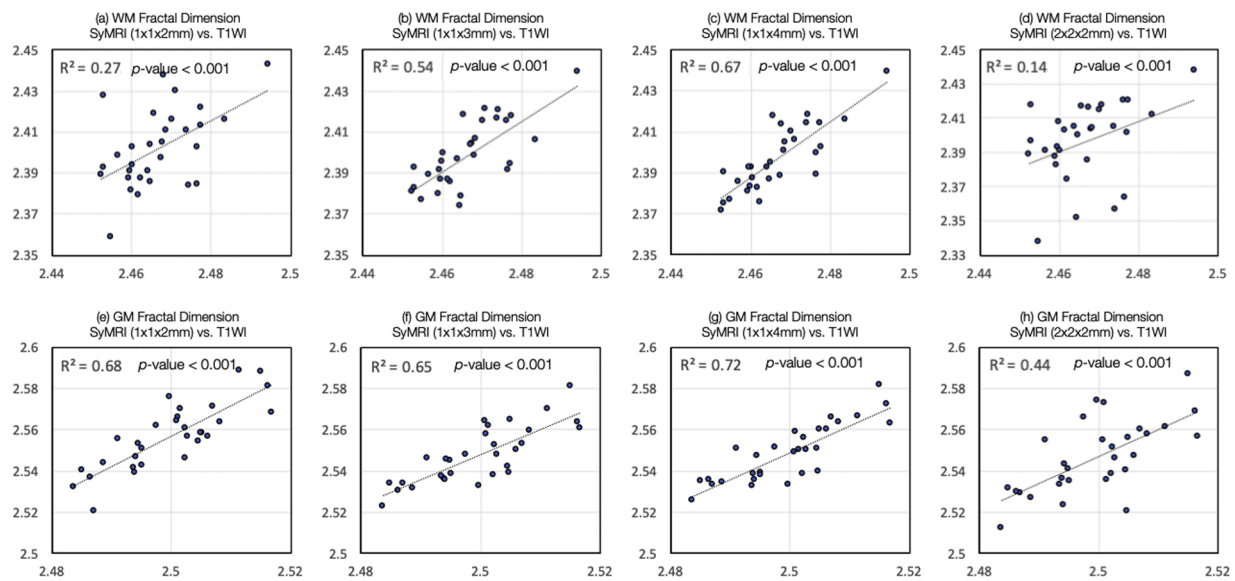


Fig. 4. Scatterplots of morphologic measurements from SyMRI compared with conventional T₁-weighted MRI. (a-d): WM-FD; (e-h): GM-FD.

the work reported in this paper.

Acknowledgements

This work was supported by an Australian National Health and Medical Research Council grant (NHMRC Early Career Fellowship 1160760); the 2019 John Mitchell Crouch Fellowship from the Royal Australasian College of Surgeons (RACS); and the Australian Research Council (ARC) Future Fellowship (2019-2023, FT190100623). We acknowledge Professor Marcel Warntjes for providing of using the SyMRI software.

References

- J. Warntjes, O.D. Leinhard, J. West, P. Lundberg, Rapid magnetic resonance quantification on the brain: optimization for clinical usage, *Mag. Reson. Med.: An Off. J. Int. Soc. Mag. Reson. Med.* 60 (2) (2008) 320–329.
- A. Hagiwara, M. Hori, J. Cohen-Adad, M. Nakazawa, Y. Suzuki, A. Kasahara, M. Horita, T. Haruyama, C. Andica, T. Maekawa, K. Kamagata, K.K. Kumamaru, O. Abe, S. Aoki, Linearity, bias, intrascanner repeatability, and interscanner reproducibility of quantitative multidynamic multiecho sequence for rapid simultaneous relaxometry at 3 T: a validation study with a standardized phantom and healthy controls, *Invest. Radiol.* 54 (1) (2019) 39–47.
- A. Hagiwara, M. Warntjes, M. Hori, C. Andica, M. Nakazawa, K.K. Kumamaru, O. Abe, S. Aoki, SyMRI of the brain: rapid quantification of relaxation rates and proton density, with synthetic MRI, automatic brain segmentation, and myelin measurement, *Invest. Radiol.* 52 (10) (2017) 647–657.
- S.M. Lee, Y.H. Choi, S.-K. You, W.K. Lee, W.H. Kim, H.J. Kim, S.Y. Lee, H. Cheon, Age-related changes in tissue value properties in children: simultaneous quantification of relaxation times and proton density using synthetic magnetic resonance imaging, *Invest. Radiol.* 53 (4) (2018) 236–245.
- M. Vagberg, T. Lindqvist, K. Ambarki, J.B. Warntjes, P. Sundstrom, R. Birgander, A. Svenningsson, Automated determination of brain parenchymal fraction in multiple sclerosis, *AJNR Am. J. Neuroradiol.* 34 (3) (2013) 498–504.
- L. Saccenti, C. Andica, A. Hagiwara, K. Yokoyama, M.Y. Takemura, S. Fujita, T. Maekawa, K. Kamagata, A. Le Berre, M. Hori, N. Hattori, S. Aoki, Brain tissue and myelin volumetric analysis in multiple sclerosis at 3T MRI with various in-plane resolutions using synthetic MRI, *Neuroradiology* 61 (11) (2019) 1219–1227.
- B.H. Menze, A. Jakab, S. Bauer, J. Kalpathy-Cramer, K. Farahani, J. Kirby, Y. Burren, N. Porz, J. Slotboom, R. Wiest, The multimodal brain tumor image segmentation benchmark (BRATS), *IEEE Trans. Med. Imaging* 34 (10) (2014) 1993–2024.
- Y. Gao, X. Xiao, B. Han, G. Li, X. Ning, D. Wang, W. Cai, R. Kikinis, S. Berkovsky, A. Di Ieva, Deep learning methodology for differentiating glioma recurrence from radiation necrosis using multimodal magnetic resonance imaging: algorithm development and validation, *JMIR Med. Inform.* 8 (11) (2020), e19805.
- A. Hagiwara, M. Hori, J. Cohen-Adad, M. Nakazawa, Y. Suzuki, A. Kasahara, M. Horita, T. Haruyama, C. Andica, T. Maekawa, Linearity, bias, intrascanner repeatability, and interscanner reproducibility of quantitative multidynamic multiecho sequence for rapid simultaneous relaxometry at 3 T: a validation study with a standardized phantom and healthy controls, *Invest. Radiol.* 54 (1) (2019) 39–47.
- M. Vågberg, K. Ambarki, T. Lindqvist, R. Birgander, A. Svenningsson, Brain parenchymal fraction in an age-stratified healthy population—determined by MRI using manual segmentation and three automated segmentation methods, *J. Neuroradiol.* 43 (6) (2016) 384–391.
- L. Pini, M. Pievani, M. Bocchetta, D. Altomare, P. Bosco, E. Cavedo, S. Galluzzi, M. Marizzoni, G.B. Frisoni, Brain atrophy in Alzheimer's Disease and aging, *Ageing Res. Rev.* 30 (2016) 25–48.
- A. Simmons, E. Westman, S. Muehlboeck, P. Mecocci, B. Vellas, M. Tsolaki, I. Kloszewska, L.O. Wahlund, H. Soininen, S. Lovestone, A. Evans, C. Spenger, MRI measures of Alzheimer's disease and the AddNeuroMed study, *Ann. N. Y. Acad. Sci.* 1180 (2009) 47–55.
- H.G. Kim, W.-J. Moon, J. Han, J.W. Choi, Quantification of myelin in children using multiparametric quantitative MRI: a pilot study, *Neuroradiology* 59 (10) (2017) 1043–1051.
- S. Fujita, A. Hagiwara, M. Hori, M. Warntjes, K. Kamagata, I. Fukunaga, M. Goto, H. Takuya, K. Takasu, C. Andica, T. Maekawa, M.Y. Takemura, R. Irie, A. Wada, M. Suzuki, S. Aoki, 3D quantitative synthetic MRI-derived cortical thickness and subcortical brain volumes: scan-rescan repeatability and comparison with conventional T(1) -weighted images, *J. Magn. Reson. Imaging* 50 (6) (2019) 1834–1842.
- M. Vågberg, K. Ambarki, T. Lindqvist, R. Birgander, A. Svenningsson, Brain parenchymal fraction in an age-stratified healthy population - determined by MRI using manual segmentation and three automated segmentation methods, *Journal of neuroradiology, J. de neuroradiologie* 43 (6) (2016) 384–391.
- S.D. Serai, J. Dudley, J.L. Leach, Comparison of whole brain segmentation and volume estimation in children and young adults using SPM and SyMRI, *Clin. Imaging* 57 (2019) 77–82.
- C. Andica, A. Hagiwara, M. Hori, M. Nakazawa, M. Goto, S. Koshino, K. Kamagata, K.K. Kumamaru, S. Aoki, Automated brain tissue and myelin volumetry based on quantitative MR imaging with various in-plane resolutions, *Journal of neuroradiology, J. de neuroradiologie* 45 (3) (2018) 164–168.
- G.B. Frisoni, A. Redolfi, D. Manset, M.-É. Rousseau, A. Toga, A.C. Evans, Virtual imaging laboratories for marker discovery in neurodegenerative diseases, *Nat. Rev. Neurol.* 7 (8) (2011) 429.
- C.R. Jack Jr., M.A. Bernstein, N.C. Fox, P. Thompson, G. Alexander, D. Harvey, B. Borowski, P.J. Britson, J.L. Whitwell, C. Ward, The Alzheimer's disease neuroimaging initiative (ADNI): MRI methods, *J. Mag. Reson. Imaging: Off. J. Int. Soc. Mag. Reson. Med.* 27 (4) (2008) 685–691.
- T. Moberget, N. Doan, D. Alnaes, T. Kaufmann, A. Córdova-Palomera, T. Lagerberg, J. Diederichsen, E. Schwarz, M. Zink, S. Eisenacher, Cerebellar volume and cerebellocerebral structural covariance in schizophrenia: a multisite mega-analysis of 983 patients and 1349 healthy controls, *Mol. Psychiatry* 23 (6) (2018) 1512–1520.
- J. West, J.B. Warntjes, P. Lundberg, Novel whole brain segmentation and volume estimation using quantitative MRI, *Eur. Radiol.* 22 (5) (2012) 998–1007.
- M. Warntjes, M. Engström, A. Tisell, P. Lundberg, Modeling the presence of myelin and edema in the brain based on multi-parametric quantitative MRI, *Front. Neurol.* 7 (2016) 16.
- A. Di Ieva, F.J. Esteban, F. Grizzi, W. Klonowski, M. Martín-Landrove, Fractals in the neurosciences, Part II: clinical applications and future perspectives, *Neuroscientist* 21 (1) (2015) 30–43.

- [24] A. Di Ieva, F. Grizzi, H. Jelinek, A.J. Pellionisz, G.A. Losa, Fractals in the neurosciences, part I: general principles and basic neurosciences, *Neuroscientist* 20 (4) (2014) 403–417.
- [25] A.D. Ieva, Erratum to: The Fractal Geometry of the Brain, Springer New York, 2016.
- [26] A. Di Ieva, P.J. Le Reste, B. Carsin-Nicol, J.C. Ferre, M.D. Cusimano, Diagnostic value of fractal analysis for the differentiation of brain tumors using 3-Tesla magnetic resonance susceptibility-weighted imaging, *Neurosurgery* 79 (6) (2016) 839–846.
- [27] F.J. Esteban, J. Sepulcre, N.V. de Mendizábal, J. Goñi, J. Navas, J.R. de Miras, B. Bejarano, J.C. Masdeu, P. Villoslada, Fractal dimension and white matter changes in multiple sclerosis, *NeuroImage* 36 (3) (2007) 543–549.
- [28] A. Di Ieva, M. Niamah, R.J. Menezes, M. Tsao, T. Krings, Y.B. Cho, M.L. Schwartz, M.D. Cusimano, Computational fractal-based analysis of brain arteriovenous malformation angioarchitecture, *Neurosurgery* 75 (1) (2014) 72–79.
- [29] S. Krohn, M. Froeling, A. Leemans, D. Ostwald, P. Villoslada, C. Finke, F.J. Esteban, Evaluation of the 3D fractal dimension as a marker of structural brain complexity in multiple-acquisition MRI, *Hum. Brain Mapp.* 40 (11) (2019) 3299–3320.
- [30] L.M. Surhone, M.T. Timpledon, S.F. Marseken, M. Sample, Wilk, Shapiro–Wilk Test, Betascript Publishing, 2010.
- [31] W.H. Kruskal, W.A. Wallis, Use of ranks in One-Criterion Variance Analysis, *Publ. Am. Stat. Assoc.* 47 (260) (1952) 583–621.
- [32] C.E. Douglas, F.A. Michael, On distribution-free multiple comparisons in the one-way analysis of variance, *Commun. Stat.* 20 (1) (1991) 127–139.
- [33] A. Traboulsee, J. Simon, L. Stone, E. Fisher, D. Jones, A. Malhotra, S. Newsome, J. Oh, D. Reich, N. Richert, Revised recommendations of the consortium of MS centers task force for a standardized MRI protocol and clinical guidelines for the diagnosis and follow-up of multiple sclerosis, *Am. J. Neuroradiol.* 37 (3) (2016) 394–401.
- [34] E. Courchesne, H.J. Chisum, J. Townsend, A. Cowles, J. Covington, B. Egaas, M. Harwood, S. Hinds, G.A. Press, Normal brain development and aging: quantitative analysis of in vivo MR imaging in healthy volunteers, *Radiology* 216 (3) (2000) 672–682.
- [35] S. Liu, W. Cai, S. Pujol, R. Kikinis, D.D. Feng, Cross-view neuroimage pattern analysis in alzheimer’s disease staging, *Front. Aging Neurosci.* 8 (2016) 23.
- [36] E. Ghione, M. Dwyer, N. Bergsland, J. Hagemeyer, D. Jakimovski, I. Paunkoski, D. Ramasamy, D. Silva, E. Carl, D. Hojnacki, C. Kolb, B. Weinstock-Guttman, R. Zivadinov, Whole brain and lateral ventricular volume changes are associated with development of disability progression in multiple sclerosis: results from a large-scale clinical routine 5-Year observational study (P3.356), *Neurology* 90 (15 Supplement) (2018). P3.356.
- [37] K.K. Mi, C.S. Hong, K. Hyeonjin, H. Moonjung, Y. Roh-Eul, Y.T. Jin, K. Ji-hoon, S. Chul-Ho, The Effect of Varying Slice Thickness and Interslice Gap on T₁ and T₂ Measured with the Multidynamic Multiecho Sequence, *Magn. Reson. Med. Sci.* (2018).
- [38] M. Jenkinson, C.F. Beckmann, T.E. Behrens, M.W. Woolrich, S.M. Smith, *Fsl*, *NeuroImage* 62 (2) (2012) 782–790.
- [39] J. Ashburner, K.J. Friston, Unified segmentation, *NeuroImage* 26 (3) (2005) 839–851.
- [40] B.B. Avants, N. Tustison, G. Song, Advanced normalization tools (ANTS), *Insight* (2008) 1–35.